RESEARCH ARTICLE

Particle & Particle Systems Characterization
www.particle-journal.com

Hydrogen and Oxygen Nanobubbles Modulate Oxidative Stress and Inflammation in Breast Cancer Cells

Helena H.W.B. Hansen, Yuao Wu, Lingxi Ouyang, Hang Thu Ta, Nam-Trung Nguyen, and Hongjie An**

Nanobubbles are an emerging and promising tool in biomedical applications, ranging from ultrasound imaging to tumor treatment. However, their physiological influences on cell health remain poorly understood. This study investigates MDA-MB-231 breast cancer cell response to varying concentrations of hydrogen and oxygen nanobubbles in relation to proliferation, intracellular reactive oxygen species (ROS) production, and inflammation. The results show that cell proliferation increases with nanobubble concentration for both hydrogen and oxygen. Hydrogen nanobubbles exhibited a stronger dose-dependent effect, whereas oxygen nanobubbles are more effective overall. Intracellular ROS production decreased with increasing nanobubble concentration for both gas types, with higher efficacy for oxygen nanobubbles. With respect to the expression of key inflammatory proteins, both nanobubble types decreased the protein expression at the highest nanobubble concentration tested, suggesting that they may suppress chronic inflammation. Finally, the wound healing assay suggested that hydrogen nanobubbles may perform better than oxygen nanobubbles with respect to cell migration. These findings suggest that nanobubble-based therapies can modulate oxidative stress and inflammation in breast cancer cells. Understanding these mechanisms will be crucial for optimizing nanobubble applications in cancer treatment and other medical fields.

1. Introduction

Nanobubbles have emerged as a versatile tool and are applied in many aspects of science, ranging from water purification[1–3] to medical imaging.[4,5] Theorists are still sceptical regarding the existence of nanobubbles due to the Epstein-Plesset calculations, which state that when a bubble decreases to the nanoscale, the external pressure is larger than the internal pressure forcing the bubble to collapse.[6] Contrary to this, experiments have shown that nanobubbles can persist for several weeks.[7] This stability is, in part, due to the presence of a surface charge, as well as their ability to stay in bulk solution as a result of their kinetic energy being greater than the effects of buoyancy.[7] Larger bubbles, i.e., microbubbles and above, are rapidly removed from the solution as their movements are governed by buoyancy. An important factor of nanobubbles is their high surface-area-to-volume ratio which making them ideal for water purification[1] and surface cleaning.[8,9] In addition, the possibility of surface modifications, along with the flexibility of the type of gas in the core, has helped nanobubbles gain traction in medical research.[10] Their surface can be engineered with stability, stealth, and targeting molecules, as well as drugs such as doxorubicin,[11] dasatinib,[12] and ibrutinib.[13] Care must be taken however, as surface modifications can make the nanobubbles easily discoverable by the immune system. In the past, polyethylene glycol (PEG) has been a prominent stealth surface modification, but recent studies have found that antidrug antibodies recognize PEG, suggesting this modification is no longer a viable option.[14,15] Therefore, using "naked" nanobubbles would be ideal as it not only removes any human-made materials that would be recognized by the immune system, but also cuts down significantly on the generation time and material costs. The gas core itself can be utilized as an imaging agent, a targeting agent or as the drug agent itself. For imaging and release of the active agent, both ultrasound and laser ablation can be used.[16] This natural multifunctionality provides an extreme amount of control over how and where the nanobubbles exhibit their function in vivo.

In medical applications, naked nanobubbles have shown promise in ultrasound imaging, as they provide a much better signal to noise ratio compared to microbubbles.[17] They are also used in the delivery of oxygen to counteract the hypoxic environment found in tumors,[18] and hydrogen nanobubbles have been applied for the removal of reactive oxygen species (ROS).[19] Another important aspect is their small size, which allows them to access areas outside the vascular system by taking advantage of the enhanced permeability and retention (EPR) effect observed in tumors.[20] Despite their current usage and ever-broadening research potential, there are still many unknowns regarding their function in vivo. Many studies tend to focus on one

H. H. Hansen, Y. Wu, L. Ouyang, H. T. Ta, N.-T. Nguyen, H. An
School of Environment and Science
Griffith University
170 Kessels Road, Nathan, QLD 4111, Australia
E-mail: nam-trung.nguyen@griffith.edu.au; hongjie.an@griffith.edu.au

The ORCID identification number(s) for the author(s) of this article can be found under https://doi.org/10.1002/ppsc.202500141

DOI: 10.1002/ppsc.202500141

aspect of nanobubbles, such as cancer treatment, without fully understanding the passive effect of nanobubbles on overall cell health. This lack of understanding is a major bottleneck within the proper usage of nanobubbles, where elucidating these reactions can assist in furthering the knowledge of how best to use them for treatment.

Nanobubbles have been studied in response to reactive oxygen scavenging. For example, hydrogen nanobubbles have been shown to function well with respect to the antioxidant defense system in a single cell system,[19] and oxygen nanobubbles have been shown to reduce hypoxia in relation to promoting topical wound healing.[21] However, it is important to note that even though these studies focus on the role of nanobubbles and ROS, these studies do not specifically look at simple cell systems. In this case, we would state that there is a critical gap in understanding how nanobubbles affect cellular processes, particularly in terms of ROS production, and by extension, inflammation regulation. A major aspect of any reaction is dependent on the concentration with too much being toxic and too little eliciting a natural build-up of immunity. The gas type is also vital as a cell's natural processes uses different gas types for different signaling pathways. Oxygen is a necessity for cell survival, and hydrogen radicals play a huge role in many important cell functions including, but not limited to, turning NAPD into NAPDH, which is essential for cell metabolism.[22] Any change in this process can be a sign of stress or disease, which can trigger an immune response or cell death. In turn, an important component of ROS is its regulation of inflammation.[23] Inadvertently triggering these responses, or preventing them, with the addition of nanobubbles for treatment of unrelated aspects could severely influence the intended treatment outcomes. In addition, triggering an unwanted inflammation response can lead to severe complications, leading to the body attacking otherwise healthy cells or preventing cell growth, causing more harm than good.[24] Gaining a better understanding of the normal reactions of nanobubbles in vitro would assist in understanding any side effects observed or why the treatment is not performing as expected, as well as finding out if off-target nanobubbles pose a threat.

This study aims to address these gaps by exploring the broader effects of nanobubbles on cell health, with a focus on ROS production, cell proliferation, and inflammation in vitro. Hydrogen and oxygen nanobubbles were generated using a mini extruder with gases produced from electrolysis. The method has been successfully used to generate nanobubbles in previous research, which offers greater control over bubble size and production volume compared to alternative methods.[25] In addition, this can be performed in a sterilized environment, protecting the cell culture from contamination.

We treated breast cancer cells with the nanobubble containing cell culture media and observed their response by assessing the cell's proliferation, intracellular ROS production, and the expression levels of vital proteins involved in the inflammatory pathway, namely IκBα and NFκB. We also performed a more visual test of cell migration/metastasis by performing a wound healing assay. A major component of oxygen nanobubble usage has been in wound healing, where it has been shown that increasing the oxygen concentration at the affected site speeds up the healing process.[21] As nanobubbles are used in other therapies related to cancer, it is of interest to understand if these nanobubbles may have an unwanted positive effect on cancer cell regeneration and metastasis.

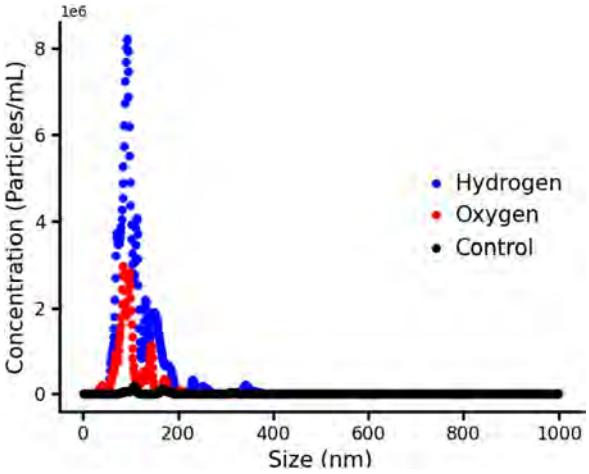

Figure 1. Nanoparticle tracking analysis of nanobubble generation using an extruder. The samples were generated in Milli-Q water. Blue: hydrogen nanobubbles, red: oxygen nanobubbles, and black: control sample (MilliQ water).

By examining the impact of nanobubble concentration and type on these key processes, this study aims to provide a deeper understanding of the potential therapeutic benefits and limitations of nanobubbles in a simple cancer cell culture system.

2. Results

2.1. Nanobubble Characterization

The generation of nanobubbles in cell culture media was achieved using a mini extruder, and their presence was proved using NTA. However, due to substantial amounts of noise caused by the presence of other materials, direct measurement of nanobubble size and concentration in the cell culture media was not possible. Instead, nanobubbles were generated in Milli-Q water. The size and concentration of the resulting nanobubbles were measured using NTA, **Figure 1**. From this figure, we observe that the control sample (black curve) has particles with an average size of 180 nm and a total particle concentration of 7.28×10^6 particles mL^{-1}. The peak value was negligible in comparison to the hydrogen and oxygen samples, as observed at 107.5 nm with a concentration of 1.81×10^5 particles mL^{-1}.

After ten cycles through the extruder with either hydrogen or oxygen gas, we observed an increase in particle concentration as well as a well-defined peak. Hydrogen nanobubbles were generated with a mean size of 114 nm and a total concentration of 3.4×10^8 particles mL^{-1}, and oxygen nanobubbles had a mean size of 97.3 nm and a total concentration of 1.03×10^8 particles mL^{-1}. The peak concentration for the hydrogen sample was 8.22×10^6 particles mL^{-1} at 91.5 nm, and for the oxygen sample, the peak concentration was 2.97×10^6 particles mL^{-1} at 83.5 nm. We noticed that, even though we used 200 nm filters, the largest peak for both samples is observed around the 100 nm mark. This

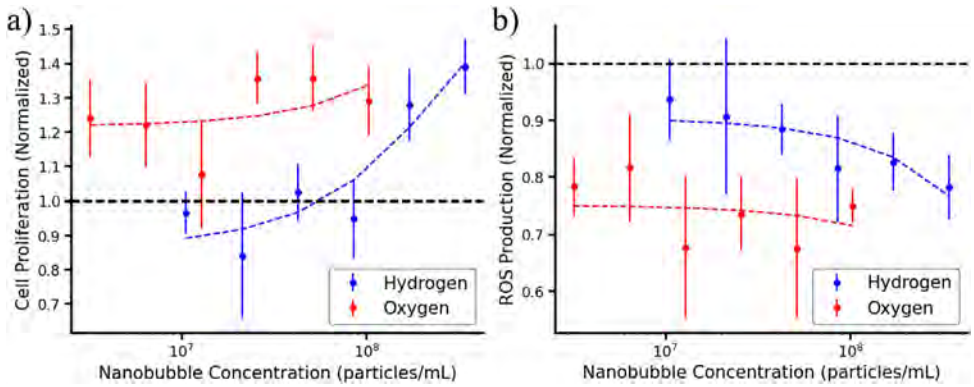

Figure 2. Cell proliferation and reactive oxygen species production in MDA-MB-231 breast cancer cells following either hydrogen or oxygen nanobubble treatment. Data was normalized with respect to the control sample, i.e., cells treated with cell culture media without nanobubbles. a) Cell proliferation of MDA-MB-231 breast cancer cells treated with cell culture media containing either oxygen (red) or hydrogen (blue) nanobubbles at different concentrations. The cell proliferation of the control sample is designated by the black dashed line in both figures. b) Intracellular ROS production in cells treated with either hydrogen nanobubbles (blue) or oxygen nanobubbles (red). Intracellular ROS production of the control sample is designated by the black dashed line. Red and blue dashed lines are a linear fit. Values are mean ± standard deviation. Representative images of the ROS fluorescence in the cell culture can be seen in Figure S1 (Supporting Information).

may be explained by the Milli-Q water being pushed through the filter at the same time as the gas, therefore not allowing the gas to expand to the edges of the pores in the filter. All the gas is not pushed through the filter at each passage due to pressure buildup in the system. The particle concentration for the control sample is negligible compared to the nanobubble samples. As the ratio of the peak and total nanobubble concentration is similar for both samples, we can assume that the gases are treated similarly by the system. Therefore, the lower concentration of oxygen nanobubbles may be due to a higher solubility of oxygen in water than hydrogen.

2.2. Effect of Nanobubbles on Cell Proliferation

The use of hydrogen and oxygen nanobubbles in cell culture is widely known, but, to our knowledge, concentration-dependent studies have not been specifically performed. With any treatment, concentration specificity is vital, which prompted us to evaluate if the cell response to nanobubbles is concentration dependent.

The first step was to gleam information regarding cell proliferation by treating MDA-MB-231 breast cancer cells with varying concentrations of nanobubbles containing cell culture media. In **Figure** 2a we show the results of the cell proliferation for a range of nanobubble concentrations. The data was normalized with respect to the control sample, cell culture media without nanobubbles, represented by the black dashed line in the figure. The concentrations were based on the original nanobubble concentrations as measured using NTA (Figure 1).

Oxygen nanobubble treatment resulted in increased cell proliferation across all concentrations. The two lowest nanobubble concentrations gave a proliferation of ≈1.23, decreasing to ≈1.07, and increasing to ≈1.35, with a cell proliferation of ≈1.29 at the highest oxygen nanobubble concentration. Our data suggests that there is a slight upward trend in cell proliferation as the oxygen nanobubble concentration increases. That the proliferation for the lowest and highest nanobubble concentrations is similar at ≈1.2 is an interesting observation, as it tells us that a lower concentration has just as much of an effect. Being able to administer lower concentrations of a drug is optimal in medicine as this lowers the chance of adverse reactions.

When treated with hydrogen nanobubbles, the cell proliferation was relative to the control samples for the four lowest concentrations of hydrogen nanobubbles with ≈0.96, ≈0.84, ≈1.02, and ≈0.95. At the two highest concentrations, the proliferation increased to ≈1.27 with a further increase to ≈1.39. The slight decrease in cell proliferation observed at the lower hydrogen nanobubble concentrations is an interesting find. This, together with the observable difference in proliferation for the oxygen samples, further cements the need for more in-depth knowledge on nanobubble concentration dependency in treatment. This is however, beyond the scope of this paper.

From the trend line, we observe that as the nanobubble concentration increases, so does the cell proliferation. The trend is less clear with respect to oxygen nanobubble treatment, where a similar reaction is observed over all the tested concentrations. In comparison, the observed trend was proportional in relation to hydrogen nanobubble concentration and cell proliferation. At lower concentrations, hydrogen treatment appears to have a minimal effect on the cell culture, and it is not until the concentration resembles that of the highest oxygen nanobubble concentration that the hydrogen nanobubbles start to have a positive impact on cell proliferation. We observe that even though the oxygen nanobubble concentration is lower than that of hydrogen, they result in similar cell proliferation at the largest tested concentration.

When comparing the hydrogen and oxygen treatment, there was no significant difference in the overall cell proliferation (p-value > 0.05). For the four lowest concentrations, apart from the third lowest, there was a significant difference between hydrogen and oxygen nanobubble treatment (p-value < 0.01), with the oxygen nanobubbles showing greater improvement. At the two highest concentrations, the proliferation of the cells was similar (p-value > 0.05) for both nanobubble types.

Together, this data suggests that oxygen treatment greatly increases cell proliferation, as supported by its use in promoting wound healing,[26] in comparison to hydrogen treatment. In addition, when considering individual nanobubble concentrations, the gas type makes a significant difference in cell proliferation. That there is no significant difference between the gases at higher concentrations may, in part, be due to oversaturation. In addition, we see that to attain a similar cell proliferation, hydrogen nanobubbles are needed at greater concentrations.

2.3. Effect of Nanobubbles on Reactive Oxygen Species

A major effect of nanobubbles in cell culture is their relation to ROS. With direct supply of hydrogen or oxygen to the cell culture, the gas may be broken down into radicals and affect the cells natural production.[27,28] We hypothesize that as the nanobubble concentration increases, the level of available gas, the intracellular ROS production would decrease as the cells can use the gas in the nanobubbles as ROS rather than generate it themselves. Figure 2b shows the level of ROS production in cell cultures at different nanobubble concentrations. When treated with hydrogen nanobubbles, the intracellular ROS production decreased with an increase in nanobubble concentration going from ≈0.93 at the lowest nanobubble concentration to ≈0.78 at the highest nanobubble concentration. In comparison, the level of ROS production when treated with oxygen nanobubbles did not shift greatly with respect to sample concentration and fluctuated between 0.68 and 0.82. A p-value < 0.01 was obtained when comparing intracellular ROS production using either hydrogen or oxygen nanobubbles over all concentrations, suggesting that gas type has a very significant effect on the level of ROS production in the cell cultures.

As with cell proliferation, we observed a greater trend in intracellular ROS production with respect to hydrogen nanobubble treatment than with oxygen nanobubble treatment. Both samples presented with an inverse proportional trend in intracellular ROS production with respect to nanobubble concentration. However, the trend is minimal, suggesting that nanobubble concentration does not have a markable effect. Gas type appears to be the deciding factor. As with cell proliferation, the largest tested nanobubble concentrations for both samples resulted in similar intracellular ROS production.

The level of cellular ROS production reflects cellular activity and the response to external stimuli and environment changes. Variations in ROS level – whether upregulation or downregulation – can give a picture of how the cells react to the presence of the nanobubbles. The observed decrease in ROS production with the increasing nanobubble concentration indicates the cells may downregulate their own ROS generation in response to the increased gas content in the cell culture media, as hypothesized. Future studies would benefit from directly measuring the level of ROS in the cell culture medium. This test would provide information on whether the gas within the nanobubbles is converted to ROS before or after uptake. Together, our cell proliferation and ROS data suggest that choosing an appropriate gas type and nanobubble concentration for treatment is crucial and non-trivial.

2.4. Western Blot for Analyzing Protein Expression

In the previous sections, we have shown that, when taking nanobubble concentration into consideration, both concentration and gas type have an impact on cell proliferation and intracellular ROS production. For this study, we chose to assess the following nanobubble concentrations: 2.58×10^7 and 1.29×10^7 particles mL^{-1} for oxygen nanobubbles, and 8.50×10^7 and 4.25×10^7 particles mL^{-1} for hydrogen nanobubbles. At the highest concentrations, the cell proliferation and intracellular ROS production were trending to be similar, so these were ignored, along with the lowest concentrations, as there was an uncertainty of the actual nanobubble concentration. At the chosen nanobubble concentrations, cell proliferation and intracellular ROS production between hydrogen and oxygen nanobubble treatment are dissimilar, which prompts us to expect distinct reactions within the cell culture. If specific reactions are reached, we will be able to observe if the hydrogen and oxygen nanobubbles initiate inflammation or anti-inflammation through similar pathways.

At an oxygen nanobubble concentration of 1.29×10^7 particles mL^{-1} and a hydrogen nanobubble concentration of 4.25×10^7 particles mL^{-1} the proliferation matched the control samples and was statistically similar across both nanobubble types (p-value > 0.05). The oxygen and hydrogen nanobubble concentrations of 2.58×10^7 and 8.50×10^7 particles mL^{-1} respectively, were chosen due to the significant difference in proliferation between the two nanobubble types (p-value < 0.01). A similar difference was observed at an oxygen nanobubble concentration of 6.44×10^6 particles mL^{-1} and a hydrogen nanobubble concentration of 2.13×10^7 particles mL^{-1}, but this was deemed a severe dilution of the original nanobubble sample, which could potentially give a large disparity in the western blot data. In addition, when looking at the level of intracellular ROS production these two samples presented with a large shift when going from an oxygen nanobubble concentration of 1.29×10^7– 2.58×10^7 particles mL^{-1}, and a hydrogen nanobubble concentration of 4.25×10^7–8.50×10^7 particles mL^{-1}. The hydrogen nanobubble sample decreased ≈0.65 where the oxygen nanobubble sample increased ≈0.6.

ROS plays a key role in the signals related to inflammation, and as we systematically managed to decrease the level of intracellular ROS production with nanobubble treatment, we decided to evaluate if this change affected the regulation of key proteins. NFκB and IκBα are important proteins in the cells response to inflammation, where NFκB activation results in direct interaction with DNA. In addition, reactive oxygen intermediates have been observed to be a common factor in NFκB signaling.[29] As NFκB forms a complex with IκBα, we chose to test these two proteins together. There are several pathways that can activate the immune response, which all include NFκB activation but do not necessarily depend on IκBα. One pathway involves the phosphorylation of IκBα, which requires oxygen, whereas the other common pathways activate NFκB in a non IκBα dependent manner. If there is an immune response, as we predict due to the introduction of ROS, we would expect the oxygen nanobubbles to use the IκBα dependent pathway, i.e., the classical pathway, whereas the hydrogen nanobubbles would use the IκBα independent pathway, i.e., the alternative pathway. The mechanisms of these two pathways

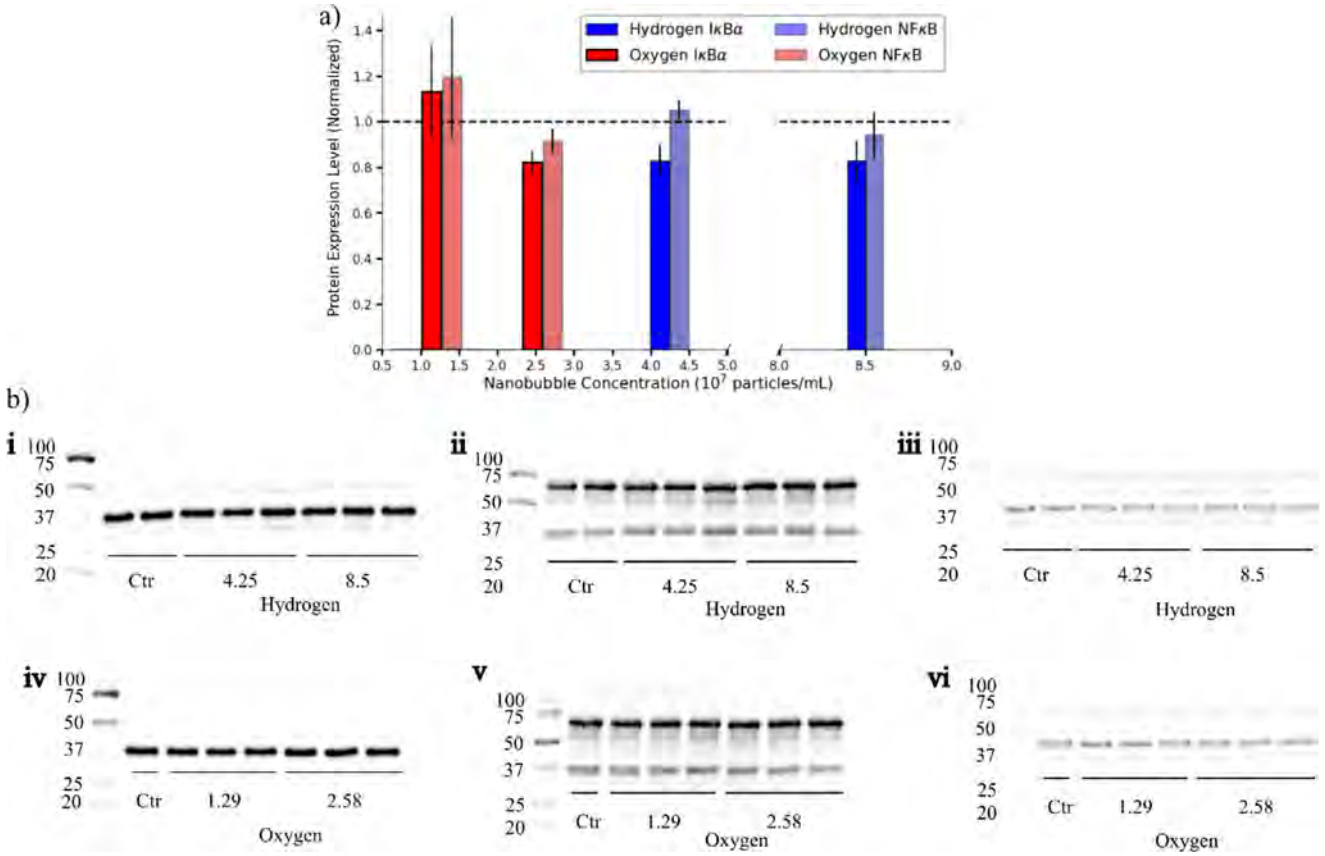

Figure 3. Protein expression of IκBα and NFκB in hydrogen or oxygen nanobubble treated MDA-MB-231 breast cancer cells. a) Quantitative data from the western blot bands. Blue: Hydrogen nanobubble treated cells, red: oxygen nanobubble treated cells, full color bars: IκBα, and shaded bars: NFκB. The graph shows representative protein levels normalized to the housekeeping protein β-actin. Experiments were performed in triplicate. Values are means ± standard deviation. b) Western blot gels. Top row (i – iii) containing two controls, the hydrogen samples at 4.25×10^7 and 8.50×10^7 particles mL^{-1}. Bottom row (iv – vi) containing one control, and the oxygen samples at 1.29×10^7 and 2.58×10^7 particles mL^{-1}. i and iv are for IκBα, ii and v are for NFκB, and iii and vi are for β-actin.

will be described further in the discussion. By assessing these two proteins, we will not only observe if the nanobubbles induce an immune response, but we will also gain insight into whether they activate similar pathways.

The antibodies used in the western blot assay are designed to bind specifically to the domain where the two proteins bind each other. Briefly, the NFκB antibody binds to the p65 domain of the protein, and the antibody for IκBα binds to the N-terminal serine region. These antibodies can therefore only bind to their respective proteins when the two are not in a complex with each other. It is noted that the IκBα antibody does not discriminate between non-phosphorylated and phosphorylated IκBα, and, as a result, the measured protein expression includes both active IκBα and IκBα that has been designated for degradation, respectively.

Figure 3 shows the data from the western blot analysis, which provides us with the expression level of NFκB and IκBα in cells treated with either hydrogen or oxygen nanobubbles. The band intensities (Figure 3b) were normalized with respect to β-actin (housekeeping protein), and the standard protein expression in control samples is represented by the horizontal dotted line in Figure 3a.

2.5. Hydrogen Nanobubble Treatment

At a concentration of 4.25×10^7 particles mL^{-1}, hydrogen nanobubble treated cell cultures had a protein expression of 0.83 ± 0.07 for IκBα and 1.05 ± 0.04 for NFκB, and at a nanobubble concentration of 8.50×10^7 particles mL^{-1}, the protein expression for IκBα and NFκB in the hydrogen-treated samples were 0.83 ± 0.09 and 0.94 ± 0.10, respectively. This data suggests an anti-inflammatory effect at the larger nanobubble concentration. For both concentrations tested, the expression of IκBα decreased, whereas NFκB expression was relatively unaffected compared to the control sample. This difference in NFκB expression, even though IκBα expression remained similar, suggests that hydrogen nanobubbles may specifically affect the former. It is possible that an inflammatory response could be initiated via the alternative pathway.

2.6. Oxygen Nanobubble Treatment

At a nanobubble concentration of 1.29×10^7 particles mL^{-1} the oxygen-treated cells had a protein expression of 1.13 ± 0.20

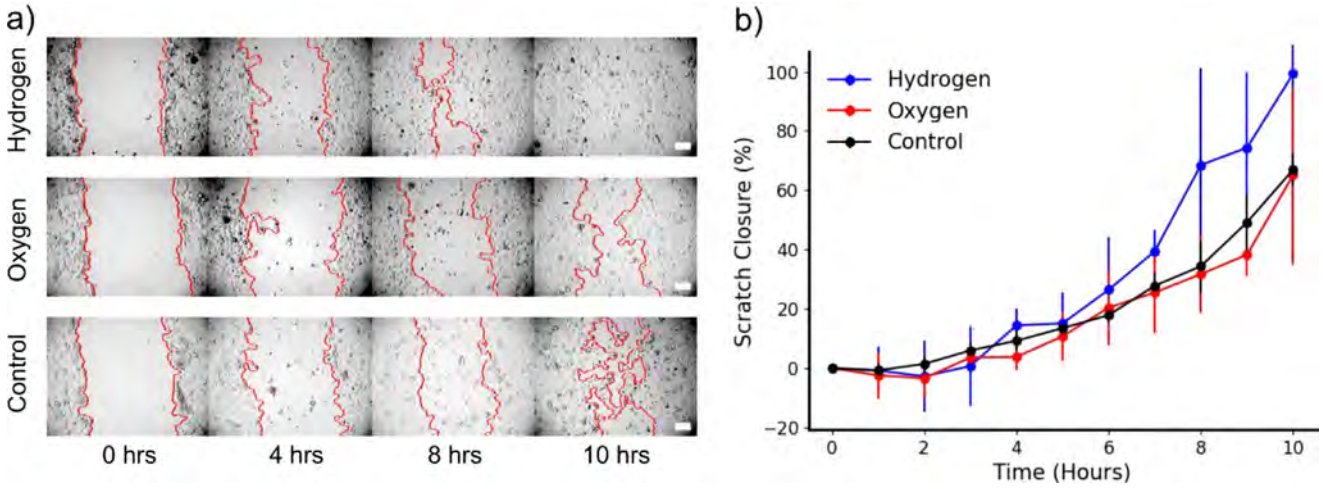

Figure 4. Wound healing assay. MDA-MB-231 cells were treated with the original solution generated for hydrogen and oxygen nanobubbles with a concentration of 3.40×10^8 particles mL^{-1}, and 1.03×10^8 particles mL^{-1}, respectively. 100% concentration of either hydrogen or oxygen nanobubbles for 24 h following a scratch made in the well plates. a) Representative images from the 10 h test are shown for each sample. The red line indicates the propagation line of the scratch edge. b) The size of the scratch was area normalized with respect to the scratch area at T_0, in addition to the nanobubble sample. As all wells were fully confluent at 24 h this data is not shown. The scale bar is 100 µm.

for IκBα and 1.19 ± 0.26 for NFκB, and 0.82 ± 0.052 for IκBα and 0.91 ± 0.05 for NFκB at a concentration of 2.58×10^7 particles mL^{-1}. By increasing the nanobubble concentration, we were able to flip the expression of both proteins, with them being under-expressed at the lower concentration, an anti-inflammatory response, and overexpressed at the higher concentration, an inflammatory response, compared to the control. This data suggests a certain level of control over cancer cells simply by controlling the amount of applied oxygen nanobubbles.

2.7. Wound Healing Assay

Cancer cells are well known for their ability to metastasize and to quickly regenerate due to their increased proliferation rate. The use of nanobubbles for cancer treatment may make treatment easier and more effective, but if a side reaction is an increase in growth, then more thought is needed regarding their usage. To study the effects of our nanobubbles on cancer cell regeneration, we performed a wound healing assay. As the cell proliferation and intracellular ROS production (Figure 2) showed comparable results with respect highest particle concentrations, we treated the cells with the highest obtainable nanobubble concentration, 3.40×10^8 particles mL^{-1} for the hydrogen nanobubble sample, and 1.03×10^8 particles mL^{-1} for the oxygen nanobubble sample. Using these conditions, we assessed whether hydrogen or oxygen nanobubbles more effectively promoted wound healing. **Figure** 4a shows representative images of the cell cultures over time, and Figure 4b depicts the scratch closure rate, where 100% means full closure. The scratch size was normalized to the initial size at T_0, when the nanobubble solution was added. The scratch was considered fully closed when no distinct wound margin remained.

Figure 4a shows representative images of the gradual healing of the scratch over the course of the first 10 h for all samples, including the control. During the initial 4 h, the closure rates for all three samples were similar. After that point, the hydrogen nanobubble treated cells sped up. Given that the media is constantly cycled through the cells, we hypothesize that there may be a concentration dependency, with the optimal concentration for the hydrogen treated samples being reached after ≈4 h. Welch's *t*-test analysis shows a *p*-value of 0.03 between the control group and the hydrogen nanobubble group, and a *p*-value of 0.37 between the control group and the oxygen group. The difference in nanobubble concentration might explain why a concentration-dependent effect for the oxygen-treated samples could require a longer time to manifest. However, over the 10-h measurement period, the oxygen-treated sample closely followed the control sample with no abrupt deviation in closure rate as observed for the hydrogen nanobubble treated sample. The scratch was fully healed in all samples at 24 h, supporting the data in Figure 2a that nanobubbles have no inherent negative effect on cell proliferation. Despite similar viability and ROS production data between the nanobubble gas types, this experiment suggests that nanobubbles may influence wound healing through different mechanisms. More research is needed to better understand the underlying effects of both nanobubble concentration and gas type in simple cancer cell systems.

3. Discussion

In this study, we treated breast cancer cells with hydrogen and oxygen nanobubbles generated using an extruder in combination with electrolysis. MDA-MB-231 breast cancer cells were treated with different concentrations of hydrogen and oxygen nanobubbles, whereafter cell proliferation and intracellular ROS production were measured, Figure 2a,b. With respect to cell proliferation, oxygen nanobubbles presented a positive effect that increased with applied concentration. This tracks with the use of oxygen nanobubbles as a wound healing treatment.[26] Hydrogen nanobubbles displayed a similar effect but to a lesser extent,

especially at lower concentrations. At the lowest concentrations tested, we even observed an adverse effect on cell proliferation. For both nanobubble types, and at all nanobubble concentrations, the intracellular ROS production decreased compared to the control, as well as presenting with a downward trend as the nanobubble concentration increased. Overall, the oxygen nanobubbles were more effective at lower concentrations.

At sufficiently high hydrogen nanobubble concentrations, the effect of both cell proliferation and intracellular ROS production became comparable. It is known that hydrogen can act as a selective antioxidant against hydroxyl radicals and neutralize ROS within the cells.[30,31] The reduction in ROS levels may result from hydrogen directly scavenging free radicals or activating intracellular antioxidant systems, thereby mitigating oxidative stress. This low oxidative stress environment may favor cell survival and proliferation. In the future, we would need to elucidate whether this observed decrease in intracellular ROS production is due to hydrogen itself antioxidant activity or if the gas within the bubbles is used by the cells, negating the need for endogenous ROS production.

The noticeable trend in cell proliferation increases in tandem with a decrease in intracellular ROS production, suggests a relationship between the two, where ROS has a negative impact on the cells. With this knowledge, together with the relationship between ROS and inflammation, we evaluated whether the nanobubbles had an anti-inflammatory effect based on the decrease in intracellular ROS production. Free radicals, i.e., reactive oxygen species, have an impact on NFκB,[32,33] and as this protein forms a complex with IκBα, we decided to test the expression levels of these two proteins.

Briefly, an inflammation response, and thereby NFκB activation, can happen in several different ways: the classical pathway, the alternate pathway, and the atypical pathway.[34] In the classical pathway, NFκB is activated via IKK phosphorylation of IκBα, whereas the alternate pathway generates the NFκB p52 protein independently of IκBα. The atypical pathway is related to UV damage, which induces IκBα degradation and is therefore independent of IKK. As we do not use UV radiation, we disregard this pathway in the following discussion. IκBα is present in the cytoplasm and binds to NFκB at its p65 domain, masking its nuclear localization. When IκBα is phosphorylated at serines 32 and 36, which are in the N-terminal domain, the protein detaches from NFκB, allowing the latter to enter the nucleus and initiate DNA transcription.[34]

Figure 3a showed that by increasing the oxygen nanobubble concentration from 1.29×10^7 to 2.58×10^7 particles mL^{-1} the cell culture went from having an increased level of the measured proteins to presenting with a decreased level compared to the control. At lower oxygen nanobubble concentration, the increase in IκBα and NFκB expression may reflect an activation of the former via the classical pathway. The overexpression of both proteins suggests the dissolution of the complex they form. That IκBα is present to a lesser extent may be due to the degradation of the protein. With an oxygen concentration of 2.58×10^7 particles mL^{-1} the expression level of both proteins decreased compared to the control, the opposite effect was observed for the lower oxygen nanobubble concentration. This suggests that at this concentration, the IκBα–NFκB complex remains intact. Together, these data present the idea that oxygen nanobubbles can induce both pro- and anti-inflammatory responses solely based on the nanobubble concentration.

The phosphorylation, and subsequent release of IκBα, requires oxygen, so we would have expected that an increase in the oxygen nanobubble concentration would have magnified the dissolution of the protein complex. Instead, we observed the opposite. This anti-inflammatory effect may be a result of the increase in cell proliferation observed in Figure 2a. When going from 1.29×10^7 to 2.58×10^7 particles mL^{-1} the cell proliferation increased from ≈1.07 to ≈1.36. The intracellular ROS production did increase as well, but only by ≈0.07. Even with the increase in oxygen nanobubble concentration and the potential for an increase in available ROS, the presence of oxygen appears to circumvent the possible phosphorylation of IκBα and instead be focused on cell growth. This concentration-dependent reaction is important to consider regarding treatment. Previously, oxygen nanobubbles have been used for wound healing, but no great care has been taken with respect to the concentration applied. We show here that, should the amount of oxygen nanobubbles that reach the affected site not be sufficient, adverse reactions may occur where the wound is exacerbated rather than treated.

Compared to oxygen nanobubbles, a change in hydrogen nanobubbles did not present with a meaningful change in protein expression. When increasing the nanobubble concentration from 4.25×10^7 to 8.50×10^7 particles mL^{-1} the concentration of IκBα stayed at ≈0.83, while the concentration of NFκB slightly decreased from ≈1.05 to ≈0.94. Our data suggests that, however slight, hydrogen nanobubbles influence NFκB expression but do not directly affect IκBα expression, indicating that at sufficiently high hydrogen nanobubble concentrations an inflammatory response may be induced via the alternate pathway. The results suggest that higher concentrations of hydrogen nanobubble may have a slight anti-inflammatory effect on the cell culture.

Overall, the decrease in unbound IκBα compared to unbound NFκB may simply be due to the high turnover rate of the protein. However, it may also be affected by the interactions between the protein and the nanobubbles due to the interfacial properties of nanobubbles, e.g., surface charges and attractive hydrophobic forces.[9] A high concentration of nanobubbles may mediate binding between unbound IκBα and NFκB. If this is the case, nanobubbles could be useful for the suppression of chronic inflammation (e.g., rheumatoid arthritis, atherosclerosis).

At all observed concentrations, oxygen nanobubbles had a positive effect on cell proliferation, whereas a negative impact was observed for the lowest hydrogen nanobubble concentrations. This suggests that by controlling the hydrogen nanobubble concentration, one would be able to tailor the response. Even though an inflammatory response may not be possible (Figure 3), one could potentially use hydrogen nanobubbles to decrease the proliferation of cancer cells. By not triggering an inflammatory response, the cells would not initiate a protective mode and would not fight the treatment. For oxygen nanobubbles, more care would be needed when choosing a relevant concentration, as an inflammatory effect can be initiated, potentially affecting the surrounding healthy cells.

Figure 4 however presents an interesting observation with hydrogen nanobubbles having an increased wound healing capacity. This effect, in combination with hydrogen's role as a selective antioxidant, brings into question whether hydrogen nanobubbles

are a desirable choice for cancer treatment. The data presented in this paper indicate that hydrogen nanobubbles have a pro-tumor effect. Enhanced cell proliferation could potentially contribute to increased tumor malignancy, while the antioxidant properties may interfere with the main targeting of oxidative stress-based therapeutic strategies used in tumor treatment. Together, these findings suggest that the use of hydrogen nanobubbles may pose a risk of treatment resistance.

For further experiments, it would be interesting to assess if we reach gas oversaturation in the cell culture at 8.50×10^7 particles mL^{-1} and above. This oversaturation could have a significant effect on the behavior of the cell culture, where the cells are better at equalizing with their environment compared to the hydrogen nanobubble concentration of 4.25×10^7 particles mL^{-1} which may be at the point where the cells react as they would normally do for external stimuli. In this way, we would also be able to search for an optimal concentration with respect to a desired outcome.

As the intracellular ROS production shows no markable change between the oxygen nanobubble concentrations (Figure 3) we cannot definitively say that ROS plays a role in the results observed for proliferation and the level of protein expression. A previous study by Zhang et al.[19] applied hydrogen nanobubbles for enhanced ROS removal, which supports our findings using nanobubbles. Reactive oxygen species have been shown to play a role in inflammation via activation of a key protein NFκB,[29] and a study by Garcia et al.[35] mentions that oxygen nanobubbles may reduce the production of harmful ROS. These studies help support our findings.

In the future we would want to decipher the reasoning behind the constant decrease in IκBα compared to NFκB observed for all tested samples, be it normal or caused by nanobubble presence. As mentioned earlier, IκBα has a fast turnover rate, and coupled with phosphorylation, this may help explain why the protein is not found at a similar concentration to NFκB. A study by Mathes et. al.[36] describes studying the different degradation pathways of IκBα and that any alteration in the IκBα degradation pathway severely dampens NFκB activation. Applying this study to our future work would give us more insight into what potential effects the different nanobubbles and their concentrations have on the tested proteins – whether their presence affects one or both proteins. Additionally, the decreased intracellular ROS production after nanobubble application is a crucial factor. In the future, testing ROS concentration in the cell culture media is necessary, as an increase here would help explain the decrease in production. Another important aspect is to study whether the down regulation of intracellular ROS production observed in this study is aiding or hindering the inflammatory response. Although no consensus has yet been reached on whether up- or downregulation is achieved with increased ROS, previous studies have continuously shown considerable overlap between the intracellular concentration of ROS and the regulation of the IκBα–NFκB complex.

Not many studies exist with respect to specifically studying wound healing or cell proliferation using nanobubbles, which makes proper data comparison difficult. In addition, many studies utilize coated nanobubbles, which introduce extra variables into the discussion. In a study by Bhavya et al.,[37] liposome encapsulated oxygen nanobubbles were applied in a similar wound healing study using MDA-MB-231 breast cancer cells. Interestingly, they showed that their nanobubble system could halt the progression of cells in a hypoxic state. In our study, we did not induce a specific state with our cells, but we showed that oxygen nanobubbles did not have a negative effect on cell growth, which indicates that there is more at play. In addition, the fact that we do not have a coating on our bubbles brings into question whether the lipid capsules safeguard the oxygen nanobubbles too well and prevent full function. Further research into the effects of naked nanobubbles and their role in cancer treatment is therefore necessary.

4. Conclusion

In this study, we treated MDA-MB-231 breast cancer cells with oxygen and hydrogen nanobubbles. Results demonstrated a positive effect on cell proliferation in a dose-dependent manner for both nanobubble types. Hydrogen nanobubbles went from having a negative effect on cell proliferation to a positive effect as the nanobubble concentration increased. In comparison, oxygen nanobubbles had a positive effect at the tested concentrations. Oxygen nanobubbles achieved better efficacy in promoting cell growth than hydrogen nanobubbles. With respect to intracellular ROS production, oxygen nanobubbles reduced ROS levels to a greater extent than hydrogen nanobubbles at all tested concentrations. Notably, with sufficiently high nanobubble concentrations, both cell proliferation and intracellular ROS production became comparable, with cell proliferation increasing as intracellular ROS production decreased. Given that ROS is a key factor in inflammation, we assessed two immune activation proteins: IκBα and NFκB. We observed that, when using oxygen nanobubbles, the cell response varied with nanobubble concentration, whereas hydrogen nanobubbles had similar reactions at both concentrations. This difference in reaction to gas type, and nanobubble concentration is an important finding necessitating more defined research into the effects of both in simple cancer cell systems.

5. Experimental Section

Chemicals and Instruments: Sodium sulphate (Chem-Supply) was used for hydrogen and oxygen gas generation via electrolysis. All chemicals for cell culture were purchased from Thermo Fisher Scientific unless otherwise stated. These included DMEM/F12 without glutamine, fetal bovine serum (FBS), penicillin-streptomycin, TrypLE express enzyme with phenol red, and trypan blue. Proliferation and reactive oxygen species were measured using resazurin sodium salt powder (Merck Life Science Pty Ltd), and 2′,7′-dichlorodihydrofluorescein diacetate (DCFH-DA, Merck Life Science Pty Ltd) respectively. Stock solutions and dilutions of chemicals were prepared in phosphate buffered saline (PBS), and negative controls that required dead cells were treated with 70% methanol prior to use.

Chemicals used for the western blot analysis included double-distilled water (ddH_2O), sodium chloride (NaCl, Chem-Supply), sodium dodecyl sulfate (SDS, Bio-Rad), 30% Acrylamide/Bis (Bio-Rad), 10% APS, TEMED (Bio-Rad), Tween 20 (Sigma), Trizma Base (Sigma), and Coles Fat Free Instant Skim Milk Powder (Coles, Australia). Several stock solutions and buffers used include: 10% SDS, 10x protease inhibitors (1 M 6-amino caproic acid, 50 mM benzamidine hydrochloride, and dH_2O. Stored at 4 °C.), running buffer (Trizma, glycine, and 10% SDS), and RIPA buffer (a mixture of Triton X100, 5 M NaCl, 1 M Tris pH 7.5, 500 mM EDTA, 250 mM

EGTA pH 9.0, 40 mM NP-40, and ddH_2O). Precision Plus Protein Kaleidoscope (Bio-Rad) was used as a weight marker for the gels, Immobilon Forte Western HRP Substrate (Millipore) was used as the detection solution for imaging, and Micro BCA TM Protein Assay Kid (Thermo Scientific) was used to measure the generation of a calibration curve to calculate the protein concentration in my samples.

The stacking and separating gels for the SDS-PAGE consisted of Tris-HCl (Trizma and HCl) buffer, 10% SDS, 30% Acrylamide/Bis, 10% APS, and TEMED. The difference was in the concentration and pH of the Tris-HCl where the stacking gel required a concentration of 0.5 M and a pH of 6.8, and the separating gel used a concentration of 1.5 M with a pH of 8.8. The gel solutions were used immediately after mixing. The Tris-HCl buffer was mixed prior to use.

The protein antibodies used for the western blot were purchased from Abcam: anti-NFκB p65 antibody, anti-IκBα antibody [E130], anti-beta actin antibody, and goat anti-rabbit IgG H&L (HRP).

Nanobubble Generation and Characterization: 0.1 M Na_2SO_4 was applied for the production of oxygen and hydrogen gas. Briefly, platinum mesh electrodes 5 mm × 5 mm (Shanghai Ledon Industrial, Co., Ltd) were placed in the solution and attached to a power source. The gas was collected and used for nanobubble generation. The mini extruder (Avanti Polar Lipid, Inc.), syringes, and filters were disinfected under UV light for 30 min prior to use. A 200 nm membrane filter (Isopore) was placed in the extruder chamber, and both syringes were inserted; one syringe contained complete cell culture media, and the other syringe contained either oxygen or hydrogen gas collected from the electrolysis. The mixture was cycled through the filter ten times, and great care was taken during the process to avoid jetting. All solutions were stored at 4 °C overnight before use to allow larger bubbles to dissipate. All nanobubble samples were used for experimentation within 24 h of generation. For control samples, untreated cell culture media was used, i.e., cell culture medium not mixed with a gas.

The size and concentration of the nanobubbles generated using the extruder were evaluated using nanoparticle tracking analysis (NTA, NanoSight NS300, Malvern Panalytical Ltd.). This method utilizes light scattering techniques to acquire precise details of particles in a disperse solution by analyzing the Brownian motion of the particles. All measurements were performed at room temperature, and data was analyzed by the NTA Analytical Software Suite. Due to the large amount of noise stemming from the cell culture media, nanobubbles generated in MilliQ water were measured instead. Double distilled water was not used as this was too clean when compared with cell culture media. As the concentration data for the NTA was given in particles/mL, the nanobubbles may be referred to as particles when specifically discussing nanobubble concentration.

Cell Culture: MDA-MB-231 human breast cancer cells (ATCC) were cultured for cell studies. The cells were treated with complete media consisting of DMEM, 10% FBS, and 1% Pen/Strep and incubated at 37 °C with 5% CO_2. For seeding in well plates, the cells were first treated with TrypLE, centrifuged at 2000 RPM for 5 min, and counted using Trypan Blue in combination with a hemocytometer. For 6-well plates, the cells were seeded at a concentration of 30 000 cells per well, and for 96-well plates, the concentration was 5000 cells per well. At 80% confluency, the cells were used for further experimentation.

The nanobubble concentration for the experiments was calculated based on the NTA results. For hydrogen nanobubbles the following concentrations were tested: 3.40×10^8, 1.70×10^8, 8.50×10^7, 4.25×10^7, 2.13×10^7, and 1.06×10^7 particles mL^{-1}. For oxygen nanobubbles the following concentrations were tested: 1.03×10^8, 5.15×10^7, 2.58×10^7, 1.29×10^7, 6.44×10^6, and 3.11×10^6 particles mL^{-1}.

Cell Proliferation: Cell proliferation was measured using Resazurin. Briefly, MDA-MD-231 breast cancer cells were seeded in a 96-well plate. The media was removed and replaced with different concentrations of the nanobubble containing cell culture media, either oxygen or hydrogen nanobubbles. Six different concentrations were tested for each nanobubble type as described in the previous section. Controls were included, which entailed treatment with plain cell culture media not containing any nanobubbles. The cells were incubated with the nanobubble sample or control solution overnight.

A 2.5 mg mL^{-1} stock solution of Resazurin in PBS was diluted a further 1000 times in PBS. The supernatant was removed from the wells and replaced with 100 µL Resazurin solution and incubated at 37 °C for 1 h. Before the addition of Resazurin, a portion of the control cells was treated with 70% methanol for background measurements. Methanol treatment kills the cells, so no proliferation occurs. Any fluorescence measured in these samples was background information and was subtracted from the fluorescence measured in wells containing live cells. The fluorescence was read using a plate reader with excitation at 535 nm and emission at 590 nm. All data were normalized with respect to the control sample.

Reactive Oxygen Species: The effect of the nanobubble solutions on the level of ROS in the cell culture was measured using DCFH-DA. MDA-MB-231 cells were seeded in 96-well plates, followed by overnight incubation with the respective nanobubble solutions as described for the proliferation study. Control samples include cells incubated with cell culture media without nanobubbles, and empty wells, i.e., no cells.

24 h after nanobubble treatment, the supernatant was removed and replaced with 100 µL of 25 µM DCFH-DA in PBS. The fluorescence was measured at an excitation of 485 and emission of 535 in a plate reader after 30 min incubation time at 37 °C. The cells were then washed with PBS and imaged using a fluorescent microscope for visual representation of ROS presence in the cells. All data were normalized with respect to the control sample.

Western Blot: MDA-MB-231 breast cancer cells were seeded in 6-well plates. The cells were treated with either hydrogen or oxygen nanobubbles, or a control solution, for 24 h. Under cold conditions, the cells were washed with PBS followed by treatment with a lysis buffer (RIPA buffer and 10X protease inhibitors) for 5 min. Using a scraper, the cells were removed from the well plates and collected in Eppendorf tubes. The samples were centrifuged at 10,000 rpm at 4 °C for 10 min, whereafter the protein-containing supernatant was collected and stored at −20 °C until further use.

The protein concentration in each sample was determined using a BCA protein assay kit. A dilution curve was generated using BSA with concentrations from 0.2 mg mL^{-1} down to 0.5 µg mL^{-1}. The supernatant of each sample collected from the cell lysis was mixed MilliQ water 1:100. The dilution curve and the protein samples were added to a 96-well plate, and all were mixed with the BSA Protein Assay Reagent 1:1 and incubated at 37 °C for 2 h. The absorbance was measured using a plate reader at 562 nm. Electrophoresis of the protein samples was done using SDS-PAGE setup from Bio-Rad. First, the gels were prepared using a separating gel with 12% acrylamide and a 4% stacking gel. The former was cast first using isopropanol to level the surface, followed by washing and addition of the latter. The gels were stored at 4 °C until use.

Using the results from the BSA protein assay in combination with the calibration curve, the protein samples were diluted to equal concentration, ≈30 µg of protein, using ddH_2O followed by the addition of the running buffer. The samples were heated to denature the proteins and subsequently loaded into the gel. A molecular weight marker was used for reference. The gels were run at 80 V followed by 120 V for 15 and 55 min, respectively. After the completed run, the protein bands were transferred from the gel to a membrane using the Bio-Rad Trans-Blot Turbo system. The gel was removed from the glass casing, placed on top of a PVDF membrane, and sandwiched between filter paper. Prior to use, the PVDF membrane was activated using ethanol, and both the membrane and filters were washed with a transfer buffer.

The membrane was used for the detection of two proteins, NFκB and IκBα, and one housekeeping protein, β-actin. The secondary antibody was IgG. For each primary antibody, the membrane was first washed with TBST (Trizma, NaCl, and Tween 20), blocked for 1 h at room temperature using 5% skim milk powder in TBST, and then incubated with the primary antibody at a 1:1000 dilution in 5% skim milk overnight at 4 °C. The day after, the membrane was washed with TBST followed by a 1 h incubation at room temperature with the secondary antibody (1:2500 in 5% skim milk). The membrane was washed again with TBST, covered in a detection solution, and imaged using a ChemiDoc imaging system. Between each primary antibody, the membrane was stripped using a stripping buffer. Analysis of

the images was done using Fiji (ImageJ), and the bands were normalized to the housekeeping protein, β-actin.

Wound Healing Assay: MDA-MB-231 cells were seeded in 6-well plates. At 80% confluency, a scratch was made in each well using a 200 µL pipette tip. Afterward the media was removed, the cells washed with HBSS, and media containing either hydrogen nanobubbles, oxygen nanobubbles, or no nanobubbles (control) were added to the wells. The scratch was imaged every hour from 0 h (addition of sample solution) to 10 h, and after 24 h. To the best of the ability, the same position in each sample was imaged every time.

Image analysis was performed with the help of Python coding. First, a binary image was generated to distinguish between covered and uncovered areas, i.e., cells and scratch area.[38] This binary image was further applied for scratch area calculations and scratch-edge detection to generate the images shown in the results. The area of the scratch over time was normalized with respect to the initial scratch area at 0 h for each sample.

Statistical Analysis: Data is represented as the mean ± the standard deviation of three independent experiments. One-way ANOVA was applied for statistical testing at a 0.05 level for cell proliferation and ROS. For the wound healing assay, Welch's *t*-test (built in Excel analysis tool, *t*-test Two-Sample Assuming Unequal Variances) was used to analyze differences between these independent groups (33 samples for each group: control group, oxygen nanobubble group, and hydrogen nanobubble.

Supporting Information

Supporting Information is available from the Wiley Online Library or from the author.

Acknowledgements

H.H. would like to thank Steen Hansen for his invaluable assistance in the development of the Python code used for data analysis. H.A. acknowledges the support from the Australian Research Council Future Fellowship (FT180100361) and the Discovery Project (DP230100556).

Conflict of Interest

The authors declare no conflict of interest.

Data Availability Statement

The data that support the findings of this study are available from the corresponding author upon reasonable request.

Keywords

anti-inflammation, cell proliferation, hydrogen nanobubbles, oxygen nanobubbles, reactive oxygen species

Received: August 24, 2025
Published online:

[1] B. Singh, N. Shukla, C.-H. Cho, B. S. Kim, M.-H. Park, K. Kim, *Toxicol. Environ. Health Sci.* **2021**, *13*, 9.
[2] A. J. Atkinson, O. G. Apul, O. Schneider, S. Garcia-Segura, P. Westerhoff, *Acc. Chem. Res.* **2019**, *52*, 1196.
[3] C. Sun, G. Wang, C. Sun, R. Liu, Z. Zhang, T. Marhaba, W. Zhang, *Water Supply* **2021**, *21*, 1608.
[4] A. A. Exner, M. C. Kolios, *Curr. Opin. Colloid Interface Sci.* **2021**, *54*, 101463.
[5] D. Wegierak, P. Nittayacharn, M. B. Cooley, F. M. Berg, T. Kosmides, D. Durig, M. C. Kolios, A. A. Exner, *Nanomed. Nanobiotechnol.* **2024**, *16*, 2007.
[6] P. S. Epstein, M. S. Plesset, *J. Chem. Phys.* **1950**, *18*, 1505.
[7] B. H. Tan, H. An, C.-D. Ohl, *Phys. Rev. Lett.* **2020**, *124*, 134503.
[8] H. H. Hansen, L. Ouyang, H. Cha, J. Zhang, Q. Li, B. H. Tan, A. Vashi, N. T. Nguyen, H. An, *ChemSusChem* **2024**, *17*, 202400802.
[9] J. Zhu, H. An, M. Alheshibri, L. Liu, P. M. Terpstra, G. Liu, V. S. Craig, *Langmuir* **2016**, *32*, 11203.
[10] H. H. Hansen, H. Cha, L. Ouyang, J. Zhang, B. Jin, H. Stratton, N.-T. Nguyen, H. An, *Biotechnol. Adv.* **2023**, *63*, 108091.
[11] F. Wang, L. Dong, S. Liang, X. Wei, Y. Wang, L. Chang, K. Guo, H. Wu, Y. Chang, Y. Yin, *Biomed. Pharmacother.* **2022**, *150*, 113042.
[12] K. K. Boddu, K. S. Gubbiyappa, *J. Drug Delivery Sci. Technol.* **2024**, *101*, 106112.
[13] M. Ponnaganti, A. K. Babu, *Nveo-Nat. Volatiles Essent. Oils J.| Nveo* **2021**, *8* , 5017.
[14] L. Hong, Z. Wang, X. Wei, J. Shi, C. Li, *J. Pharmacol. Toxicol. Methods* **2020**, *102*, 106678.
[15] B. Pezeshkpoor, N. Sereda, A.-C. Berkemeier, I. Matuschek, N. Schwarz, P. L. Turecek, S. Horneff, C. Klein, G. Goldmann, N. Marquardt, *J. Thromb. Haemostasis* **2023**, *21*, 1503.
[16] Q. Xiao, Q. Jia, M. Inam, Q. Chen, X. Sun, *Med. Gas Res.* **2025**, *15* , 214.
[17] B. Helfield, Y. Zou, N. Matsuura, *Front. Phys.* **2021**, *9*, 654374.
[18] J. Owen, K. Logan, H. Nesbitt, S. Able, A. Vasilyeva, E. Bluemke, V. Kersemans, S. Smart, K. A. Vallis, A. P. McHale, *Nano Select* **2022**, *3*, 394.
[19] Y. Zhang, W. Fan, X. Li, W.-X. Wang, S. Liu, *Environ. Sci. Technol.* **2022**, *56*, 15096.
[20] D. V. Batchelor, R. H. Abou-Saleh, P. L. Coletta, J. R. McLaughlan, S. A. Peyman, S. D. Evans, *ACS Appl. Mater. Interfaces* **2020**, *12*, 29085.
[21] X. Han, L. Ju, C. Saengow, W. Ren, R. Ewoldt, T. Fan, J. Irudayaraj, *Bioact. Mater.* **2024**, *35*, 67.
[22] M. E. Migaud, M. Ziegler, J. A. Baur, *Nat. Rev. Mol. Cell Biol.* **2024**, *25*, 822.
[23] J. Liu, X. Han, T. Zhang, K. Tian, Z. Li, F. Luo, *J. Hematol. Oncol.* **2023**, *16*, 116.
[24] L. Zuo, D. Wijegunawardana, *Lung Inflammation Health Dis.* **2021**, *II*, 187.
[25] L. Ouyang, H. H. Hansen, H. Cha, X. Ji, J. Zhang, Q. Li, B. H. Tan, Q. T. Trinh, N.-T. Nguyen, H. An, *Colloids Surf. A* **2024**, *700*, 134773.
[26] L. R. Sayadi, D. A. Banyard, M. E. Ziegler, Z. Obagi, J. Prussak, M. J. Klopfer, G. R. Evans, A. D. Widgerow, *Int. Wound J.* **2018**, *15*, 363.
[27] C. A. Juan, J. M. Pérez de la Lastra, F. J. Plou, E. Pérez-Lebeña, *Int. J. Mol. Sci.* **2021**, *22*, 4642.
[28] A. J. P. O. de Almeida, J. C. P. L. de Oliveira, L. V. da Silva Pontes, J. F. de Souza Júnior, T. A. F. Gonçalves, S. H. Dantas, M. S. de Almeida Feitosa, A. O. Silva, I. A. de Medeiros, *Oxid. Med. Cell. Longevity* **2022**, *2022*, 1225578.
[29] B. Kaltschmidt, T. Sparna, C. Kaltschmidt, *Antioxid. Redox Signaling* **1999**, *1*, 129.
[30] J. Slezak, B. Kura, T. W. LeBaron, P. K. Singal, J. Buday, M. Barancik, *Curr. Pharm. Des.* **2021**, *27*, 610.
[31] S.-i. Hirano, Y. Ichikawa, B. Sato, H. Yamamoto, Y. Takefuji, F. Satoh, *Int. J. Mol. Sci.* **2021**, *22*, 4566.
[32] A. Siomek, *Acta Biochim. Pol.* **2012**, *59*, 323.
[33] K. Lingappan, *Curr. Opin. Toxicol.* **2018**, *7*, 81.

[34] Q. Guo, Y. Jin, X. Chen, X. Ye, X. Shen, M. Lin, C. Zeng, T. Zhou, J. Zhang, *Signal Transduction Targeted Ther.* **2024**, *9*, 53.
[35] S. M. V. Garcia, M. S. Khan, Z. S. Haidar, J. P. Acevedo Cox, *Nanomaterials* **2023**, *13*, 3060.
[36] E. Mathes, E. L. O'dea, A. Hoffmann, G. Ghosh, *EMBO J.* **2008**, *27*, 1357.
[37] K. Bhavya, K. Agarwal, D. Negi, K. Niveria, Y. Singh, A. K. Verma, S. Dasgupta, N. Nirmalkar, D. Pal, *ACS Appl. Nano Mater.* **2024**, *7*, 25198.
[38] S. Bhattiprolu, python_for_microscopists. https://github.com/bnsreenu/python_for_microscopists/blob/master/021-scratch_assay_using_scikit_image.py (accessed: 2024 June).

Supplementary Material

Hydrogen and oxygen nanobubbles modulate oxidative stress and inflammation in breast cancer cells

Helena H.W.B. Hansen [a], Yuao Wu [a], Lingxi Ouyang [a], Hang Thu Ta [a], Nam-Trung Nguyen [a*], and Hongjie An[a*]

[a] School of Environment and Science, Griffith University, 170 Kessels Road, Nathan, QLD 4111, Australia

*Corresponding author

Email: hongjie.an@griffith.edu.au, nam-trung.nguyen@griffith.edu.au

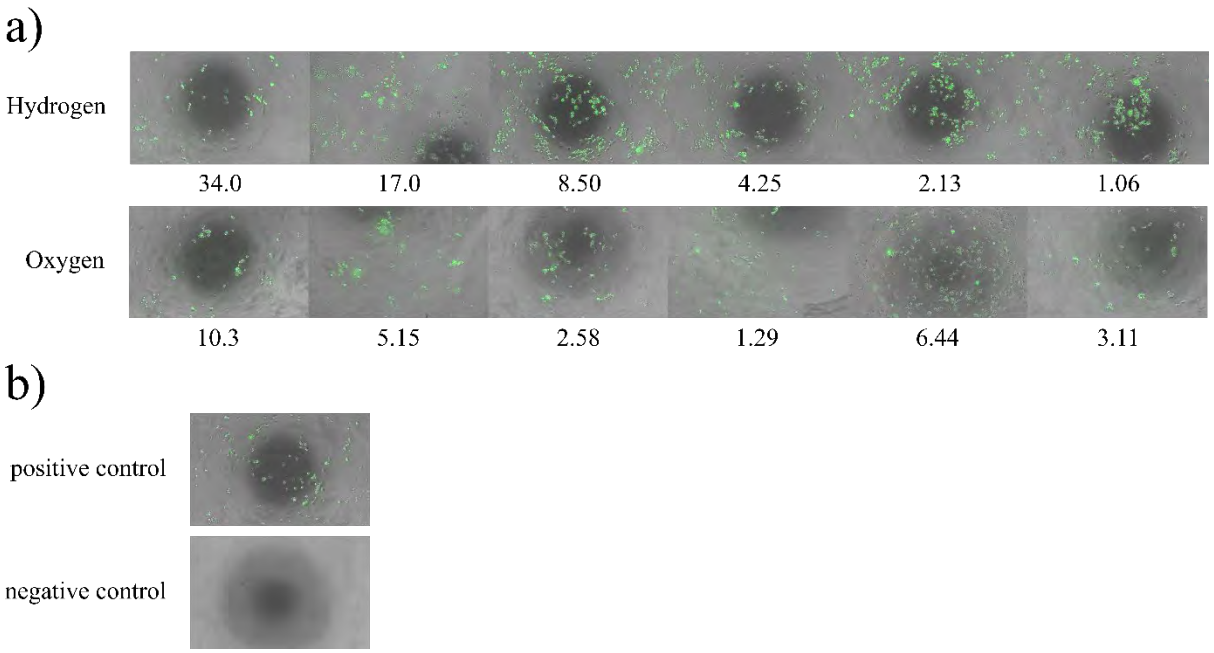

Figure S1. Representative images of the ROS fluorescence for a) hydrogen and oxygen nanobubbles, and b) positive (control cells, i.e. plain cell culture media) and negative (no cells) control. The numbers in a) represent the nanobubble concentration in each sample as a function of 10^7 particles/mL corresponding to the ROS data shown in Figure 2.